# Structural Transitions and Melting in $LJ_{74-78}$ Lennard-Jones Clusters from Adaptive Exchange Monte Carlo Simulations†

**Vladimir A. Mandelshtam* and Pavel A. Frantsuzov**

*Chemistry Department, University of California at Irvine, Irvine, California 92697*

**Florent Calvo**

*Laboratoire de Physique Quantique, IRSAMC, Université Paul Sabatier, 118 Route de Narbonne, F31062 Toulouse Cedex 9, France*

*Received: October 12, 2005; In Final Form: November 10, 2005*

Phase changes in Lennard-Jones (LJ) clusters containing between 74 and 78 atoms are investigated by means of exchange Monte Carlo simulations in the canonical ensemble. The replica temperatures are self-adapted to facilitate the convergence. Although the 74- and 78-atom clusters have icosahedral global minima, the clusters with 75−77 atoms have decahedral ground-state structures and they undergo a structural transition to icosahedral minima before melting. The structural transitions are characterized by quenching and by looking at the $Q_4$ and $Q_6$ orientational bond order parameters. The transition temperatures are estimated to be 0.114, 0.065, and 0.074 reduced units for $LJ_{75}$, $LJ_{76}$, and $LJ_{77}$, respectively. These values, their ordering and the associated latent heats are compared with other estimates based on the harmonic superposition approach.

## I. Introduction

Atomic clusters display very rich structural, thermal and dynamical properties.[1−3] The large surface/volume ratio of these objects make them particularly useful in fields such as catalysis or optoelectronics, to name a few. Clusters are different from bulk matter in many respects, because their behavior evolves as they grow. Physical and chemical quantities vary with the number of constituents, sometimes nonmonotonically. In some cases such as mercury or magnesium, the nature of chemical bonding itself depends on the size of the system.

Clusters bound by the simple pairwise Lennard-Jones (LJ) potential have been of considerable interest for theoreticians. Despite their chemical simplicity, the wide range of unusual phenomena they display make them particularly valuable for understanding the general rules underlying structure and phase transitions in small systems. More practically, they are still regularly used as a benchmark to design new algorithms for global optimization, ergodic sampling, and more recently to construct reaction pathways and to estimate the related rate constants.[4]

Though most of Lennard-Jones clusters show lowest-energy structures with icosahedral symmetry (until about 1000 atoms are reached), close-packed shapes may be found when perfect or nearly perfect geometric arrangements (the so-called magic numbers) with filled atomic shells are possible. Such a situation occurs in the 38-atom cluster $LJ_{38}$, which is characterized by a truncated octahedral global energy minimum.[5] Because many icosahedral structures are only marginally higher in energy, the energy landscape of $LJ_{38}$ can be described in terms of two funnels[6] corresponding to the cubic or icosahedral isomers, respectively. Due to its higher entropy, the icosahedral funnel dominates over truncated octahedral structures at moderate temperatures, before melting. This structural transition is very hard to simulate directly, because the free energy barrier is large,[6] resulting in extremely slow crossing events. This problem, referred to as broken ergodicity, may occur for any system with a complex energy landscape[7] such as structural glasses or biomolecules.

Broken ergodicity is a trouble for most conventional simulation algorithms. It also affects the physical or chemical properties of interest that highly depend on a correct sampling of the important regions of the energy landscape. Among the many methods that have been proposed in the past decades to reduce broken ergodicity and slow convergence, the exchange Monte Carlo (EMC) method (also known as parallel tempering or replica-exchange) has become a standard tool.[8,9] In its basic form EMC involves running a series of simultaneous trajectories at several temperatures, which occasionally communicate with each other and attempt to swap configurations. Kinetic trapping is avoided by allowing the low-temperature configurations to be suddenly heated by jumping to higher temperatures.

The EMC method has been used successfully in many studies on clusters in the past,[10−16] including specific applications to $LJ_{38}$.[10,11,17−19]

Depending on the structure of the global minimum, a LJ cluster may undergo one or more structural transformations according to the following general rules. Below size 31, the ground-state geometry is based on the polyicosahedral or anti-Mackay motif. At size 31 and above, clusters with Mackay icosahedral layers are favored. For the three-layer clusters the corresponding critical size is 82, so that clusters above 82 (except $LJ_{85}$) have Mackay overlayers. At some finite temperature such clusters undergo the surface transition to the anti-Mackay phase, as the latter is entropically more favorable than the former.[16,20] In particular, $LJ_{31}$ shows a Mackay to anti-Mackay transition at very low temperature ($T \simeq 0.03\ \epsilon/k_B$).[20,21] The temperature-induced Mackay to anti-Mackay transition becomes more pronounced with increasing size.

† Part of the special issue "John C. Light Festschrift".

10.1021/jp055839l CCC: $33.50 
Published on Web 12/23/2005

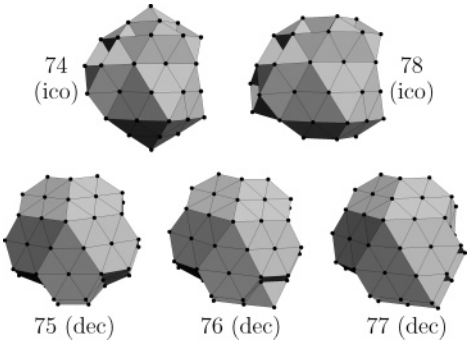


**Figure 1.** Lowest-energy minima of $LJ_n$ clusters, $n = 74-78$. The icosahedral (ico) and decahedral (dec) shapes are indicated.

Melting of the core of the cluster occurs at higher temperatures[16] but is not always easy to characterize, especially for clusters with $n < 55$ for which the core consists of only 13 atoms.

Clusters with nonicosahedral global minima are expected to undergo low-temperature solid−solid transitions to the icosahedral local minima, because the latter are entropically more favorable than the former. The most well studied of those special cases is $LJ_{38}$, for which the heat capacity curve shows a clear shoulder near the solid−solid transition temperature $T_{ss} = 0.12$ $\epsilon/k_B$, as well as a sharp melting peak at near $T = 0.17$ $\epsilon/k_B$. An earlier work[22] based on alternative estimates from the superposition of inherent structures[23] predicts similar behavior for the heat capacity curve of $LJ_{38}$, although the shoulder at the solid−solid transition is replaced by a distinct peak. In the present work, we focus on sizes close to 75, which is the next special case after 38. The lowest-energy minima of $LJ_n$ clusters with $n = 75-77$ are all based on Marks decahedra, with one or two extra atoms in the cases of $LJ_{76}$ or $LJ_{77}$, respectively. Conversely, the 74- and 78-atom clusters are icosahedral, with an incomplete anti-Mackay overlayer surrounding the two-layer Mackay icosahedron. In the case of $LJ_{78}$, the most stable arrangement is found by removing a vertex atom from the Mackay icosahedron. The structures of the global minima of $LJ_n$ clusters, $n = 74-78$, are depicted in Figure 1.

Because the energy landscape of $LJ_{75}$ also has two main funnels,[21] and because the narrowest (decahedral) funnel is also the deepest, a structural transition toward the icosahedral funnel is expected at low temperatures, similar to what occurs in $LJ_{38}$. The two other clusters with decahedral global minima, at $n = 76$ and 77, are expected to have a double-funnel energy landscape as well, whereas $LJ_{74}$ and $LJ_{78}$ have single-funnel landscapes. Up to now, thermal effects in the $LJ_n$ clusters with $n$ close to 75 have been only addressed using the harmonic superposition approach.[24,25] These calculations predict that the solid−solid transition occurs at $T_{ss} = 0.082$, 0.046, and 0.048 reduced units for $n = 75$, 76, and 77, respectively.[24,25] Although they rely on sampling tens of thousands of minima, the superposition calculations are based on several assumptions that can affect the transition temperatures, mainly the weighting corrections and the harmonic approximation for the individual densities of states. Our goal here is to provide a detailed numerical simulation of the phase changes in the $LJ_n$ clusters with $74 \le n \le 78$ using extensive Monte Carlo simulations. As was the case for $LJ_{38}$, the EMC strategy turns out to be essential such that convergence can be eventually reached at temperatures close to the structural transition. A suitable analysis of the thermodynamical effects requires looking at some order parameters. Here the bond orientational order parameters $Q_4$ and $Q_6$ introduced by Steinhardt and co-workers[26] are used to distinguish icosahedral and decahedral isomers from each other. Systematic quenching also helps to relate the simulation results to the main features of the energy landscape, namely its local minima.

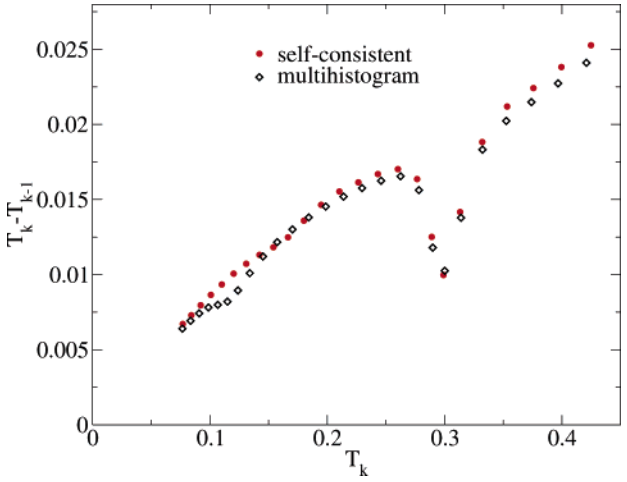


**Figure 2.** Full symbols: optimized temperature grid (in reduced units $\epsilon/k_B$) used in the present work for the $LJ_{75}$ cluster. It was obtained self-consistently during the first $10^9$ MC steps with the constraint that the mean exchange rate between replicas with adjacent temperatures $T_k$ and $T_{k-1}$ was 50%. Open symbols: multiple-histogram estimate of an optimal temperature grid obtained after the equilibrium had been reached.

The paper is organized as follows. In the next section, we briefly describe the exchange Monte Carlo method employed in the present work, and we emphasize the procedure used to find the optimal location of replicas that lead to a constant chance of swapping configurations. Our main results are given in section 3. In particular we calculate the two-dimensional probability distribution function of both temperature and the $Q_4$ or $Q_6$ order parameters. We also discuss the dependence of our estimated transition temperatures with respect to the equilibration and averaging statistics. We finally summarize and conclude in section 4.

## II. Exchange Monte Carlo Simulations

For each cluster size an EMC calculation was carried out on a single Opteron processor and took several months of CPU time. The algorithm implementation was similar to that described in ref 10, except for the choice of the set of replica temperatures $T_1 < T_2 < ... < T_K$. The optimal allocation of temperatures in canonical exchange Monte Carlo simulations has been the subject of previous investigations.[27−32] More precisely, the goal is that the mean exchange rate between replicas with adjacent temperatures $T_k$ and $T_{k+1}$ is about 50% and remains approximately constant with $k$. In the present work the temperature schedule was chosen self-consistently following the procedure described by Hukushima and Nemoto.[33] During this self-consistent calculation $T_1$ was set equal to the lowest temperature of interest $T_{min}$, whereas the total number of replicas $K$ was determined from the condition $T_K \ge T_{max}$ with $T_{max} \approx 0.42$, which is sufficiently large for the Metropolis random walk to sample the configuration space efficiently. The full symbols in Figure 2 show the optimized grid actually used for the $LJ_{75}$ cluster. It was obtained during the first $10^9$ MC steps. Relative to the main calculation, the running time needed for grid optimization is negligible, whereas the gain due to acceleration of the convergence may be substantial. Moreover, because the grid optimization actually contributes to the equilibration, no numerical effort is wasted. The optimal schedule is essentially

geometric, except near the melting point, $T \sim 0.3$, where an accumulation is observed. Note that it does not reproduce correctly the small dip near the solid−solid transition at $T \sim 0.1$ seen in the temperature schedule, optimized by the multiple-histogram method (see below) but after the equilibrium had been reached (open symbols). This, however, should have no noticeable effect on the convergence of the EMC calculation.

For all $n$ we implemented a hard constraining sphere with radius $R = 3.5\sigma$ to prevent cluster dissociation. The swaps of configurations between the random walks with adjacent temperatures were attempted every once in 100 MC steps per temperature, where one MC step corresponds to an attempt to move one of the atoms using the Metropolis scheme.

Also, we took the advantage of the knowledge of the global minima configurations[34] and used them as initial configurations for all the random walks. We believe that 1 order of magnitude longer equilibration times could be needed without the special choice of the initial configuration. The reason is that the global minima, at least for $LJ_{75-77}$, belong to a very narrow funnel of the potential energy landscape and are extremely hard to find by a Monte Carlo search.

The heat capacities were computed using the standard fluctuation formula

$$C_V(T) = \frac{3nk_B}{2} + \frac{1}{k_B T^2}(\langle E^2\rangle_T - \langle E\rangle_T^2) \tag{1}$$

The canonical averages between the replica temperatures ($T_k < T < T_{k+1}$) were interpolated using the following expression

$$\langle A\rangle_T \approx \alpha_k(T)A_k(T) + [1 - \alpha_k(T)]A_{k+1}(T) \tag{2}$$

where

$$\alpha_k(T) = \cos^2\left[\frac{\pi(T - T_k)}{2(T_{k+1} - T_k)}\right]$$

and

$$A_k(T) = \frac{1}{N_{MC}}\sum_{n=1}^{N_{MC}} \exp[(\beta_k - \beta)E(q_n^{(k)})]A(q_n^{(k)}) \tag{3}$$

with the sequence of configurations $\{q_n^{(k)}\}$ ($n = 1, ..., N_{MC}$) generated by a Metropolis random walk at temperature $T_k$, where $\beta = 1/k_B T$ defines the inverse temperature. Note that in principle (eq 3) alone gives an exact expression for $\langle A\rangle_T$ for any $T$ and $T_k$ in the $N_{MC} \to \infty$ limit. However, practically, it can be used only when the difference $T - T_k$ is not too large; otherwise, its numerical convergence is very poor.

In each EMC calculation the energy moments $\langle E\rangle_T$ and $\langle E^2\rangle_T$ were partially averaged and recorded after every $N_{MC} = 5 \times 10^7$ MC steps per temperature. The convergence was then monitored by comparing results obtained from independent runs. As demonstrated in Figure 7, even with the smart choice for the initial configurations the equilibration time for $LJ_{75}$ is still quite long, $\sim 10^{10}$ MC steps per temperature, and is even longer for the two other clusters ($LJ_{76,\ 77}$) with decahedral global minima.

Alternatively, the caloric curve can be reconstructed from the distribution of potential energies gathered from all trajectories, using a multiple-histogram reweighting procedure.[35] We performed such a calculation for $LJ_{75}$, but the heat capacities using this least-squares fitting procedure and the interpolating scheme turned out to be very close. In addition to the interpolation, the multiple-histogram procedure provides the microcanonical density of states (DOS) $\Omega(E)$, which can be used in turn to calculate an optimal temperature schedule. Having set one temperature $T = 1/k_B\beta$, the optimal next temperature $T' = 1/k_B\beta'$ can be estimated from the average chance of accepting an exchange, given exactly by

$$\langle p(T,T')\rangle = \frac{1}{Z(\beta)\,Z(\beta')}\int\int dE\, dE'\, \Omega(E)\, \Omega(E') \times \min[1,\exp(\Delta\beta\Delta E)]\, \exp(-\beta E - \beta' E') \tag{4}$$

In the previous equation, we have used the notations $\Delta\beta = \beta - \beta'$ and $\Delta E = E - E'$, and $Z(\beta)$ is the partition function at inverse temperature $\beta$:

$$Z(\beta) = \int \Omega(E) \exp(-\beta E)\, dE \tag{5}$$

By solving numerically the equation $\langle p(T, T')\rangle = 0.5$ for $T' > T$, and by repeating the calculation iteratively, we can find the optimal allocation of temperatures. The repartition obtained from our estimate of the DOS for $LJ_{75}$, also represented in Figure 2, matches well the repartition obtained on the fly.

To interpret the caloric curve of $LJ_{75}$, periodic quenches have been performed for each trajectory to probe the important parts of the energy landscape. The $Q_4$ and $Q_6$ orientational bond order parameters have been calculated not only on the fly but also for quenched configurations. At each temperature, the probability distributions of $Q_4$ and $Q_6$ were also calculated.

## III. Results and Discussion

The heat capacities of the five LJ clusters are represented in Figure 3a. The curves have been vertically shifted for a better visualization. Except at low temperature $T < 0.2$, they all show a main peak centered near $0.295\ \epsilon/k_B$. The peaks signal the onset of the solid−liquid transition. Extra calculations performed in the microcanonical ensemble show that the kinetic temperature exhibits a S-bend. This result is confirmed by looking at the distribution of potential energies, which is bimodal at the melting point.[36]

The latent heat of melting have been estimated from the area under the main heat capacity peak. Both the melting temperature and the latent heat ($0.20\ \epsilon$/atom) remain rather constant in this size range. The low-temperature behavior is much more interesting, as it emphasizes strong cluster size effects. The heat capacities of the $LJ_{75-77}$ clusters exhibit extra peaks that are best seen in Figure 3b.

Even though icosahedral clusters may also undergo isomerization and premelting effects (an illustration is found on $LJ_{58}$[16]), we have not found any bump or shoulder in the heat capacities of $LJ_{74}$ or $LJ_{78}$. Instead, clusters with a decahedral ground-state structure exhibit well-defined peaks centered at the temperatures 0.114, 0.064, and 0.074 (in reduced units $\epsilon/k_B$) for clusters with increasing size. It is worthwhile to notice that the heat capacity grows faster than linearly at temperatures higher than the peak center. This indicates that anharmonicities are significant.[37] Periodic quenches performed at the low-temperature replicas show that icosahedral isomers are visited already at $T = 0.07\epsilon/k_B$, even though they are in very small proportions (about 1/2000). This is a good indication that the parallel tempering procedure was successful in the present case.

The averages $\langle Q_4\rangle$ and $\langle Q_6\rangle$ of the bond orientational order parameters are represented in Figure 4 for $LJ_{75}$ as a function of increasing temperature. We considered the values obtained from instantaneous configurations taken on the fly, as well as those

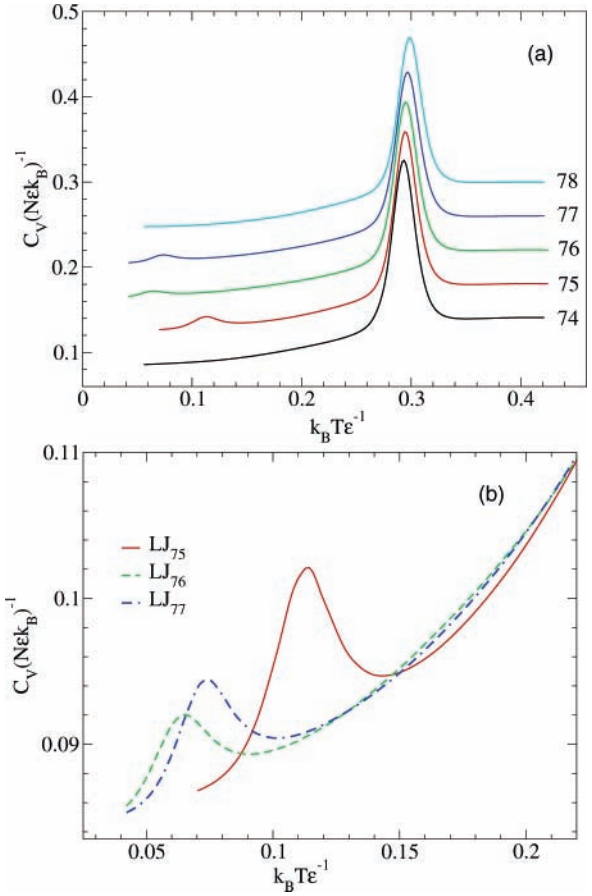


**Figure 3.** (a) Heat capacities for the LJ clusters with five consecutive sizes ($n = 74-78$). For better presentation each curve was shifted up by 0.04 ($n - 74$). For $LJ_{75-77}$ the averages were collected over $1.5 \times 10^{10}$ MC steps per temperature after $10^{10}$ equilibration steps, whereas for $LJ_{74,78}$ the averaging was performed using only $5 \times 10^9$ steps with $5 \times 10^9$ equilibration steps. (b) Low-temperature region where the solid−solid transition for $LJ_{75-77}$ occurs. (Here the curves are not shifted.)

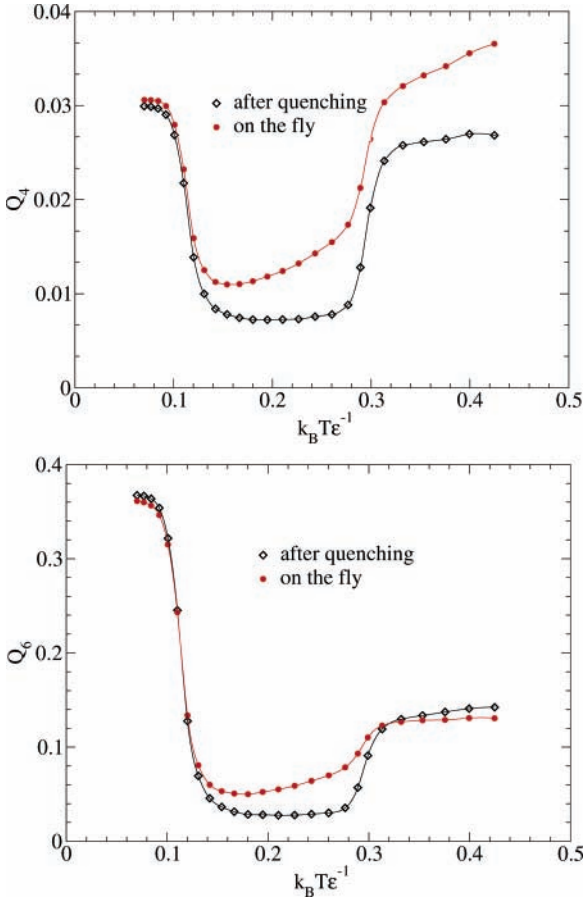


**Figure 4.** Mean values $\langle Q_4 \rangle_T$ and $\langle Q_6 \rangle_T$ of the order parameters as a function of temperature for the $LJ_{75}$ cluster averaged over the quenched and instantaneous configurations. The continuous curves were obtained by interpolation between the temperature grid points.

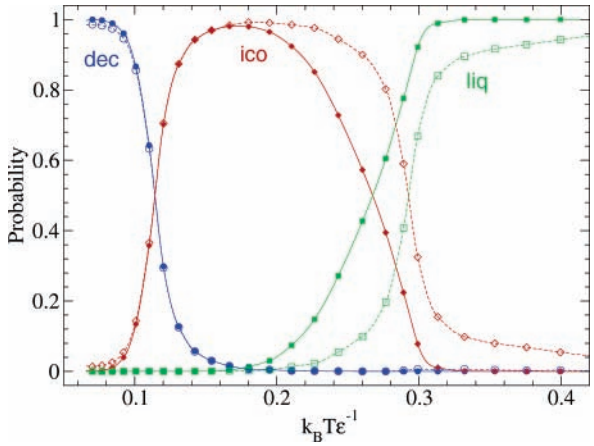


**Figure 5.** Probabilities to observe decahedral, icosahedral and liquidlike structures as a function of temperature for the $LJ_{75}$ cluster obtained from quenching the equilibrium configurations using the energy criteria (full symbols) or $Q_4$ and $Q_6$ order parameters (open symbols). The continuous curves were obtained by interpolation between the temperature grid points.

after quenching to reduce thermal fluctuations. From Figure 4 $Q_4$ may not seem as a good order parameter, because its value in the decahedral ground-state structure is already rather low ($<0.04$). Conversely $Q_6$ has a relatively high value in the decahedral isomer, close to 0.3. As temperature crosses 0.11, the strong decrease in both $Q_4$ and $Q_6$ suggests that other structures with icosahedral local order becomes favored over the decahedral global minimum.

Interestingly, the two order parameters exhibit another sharp variation at the melting point. In addition, quenching does not significantly affect the value of $Q_4$ or $Q_6$. Therefore, the liquidlike isomers found at temperatures higher than $T = 0.3$ contribute to increasing the local order with respect to the icosahedral isomers for which the order parameters are minimized.

The simplified energy landscape of $LJ_{75}$ investigated by Doye, Miller, and Wales[21] clearly shows a double-funnel shape. Although the funnel with local minima having a Mackay overlayer is not favored at any temperatures in the case of $LJ_{75}$, this picture is qualitatively similar to that in $LJ_{38}$ but quantitatively much worse: the larger energy barrier, which separates the two major funnels, as well as the increase of the density of states, due to the increase of the dimensionality of the system, both contribute to the increase of the correlation time in the EMC simulation.

On the basis of ref 21, we distinguish three classes of isomers depending on the potential energy $E$ of a given inherent structure, corresponding to the decahedral funnel only ($E < -397\ \epsilon$), the icosahedral funnel ($-397\ \epsilon \le E < -394\ \epsilon$), and the remaining liquidlike isomers ($E \ge -394\ \epsilon$). Such a definition for the classes leads to the probabilities as a function of temperature shown in Figure 5 using the solid symbols.

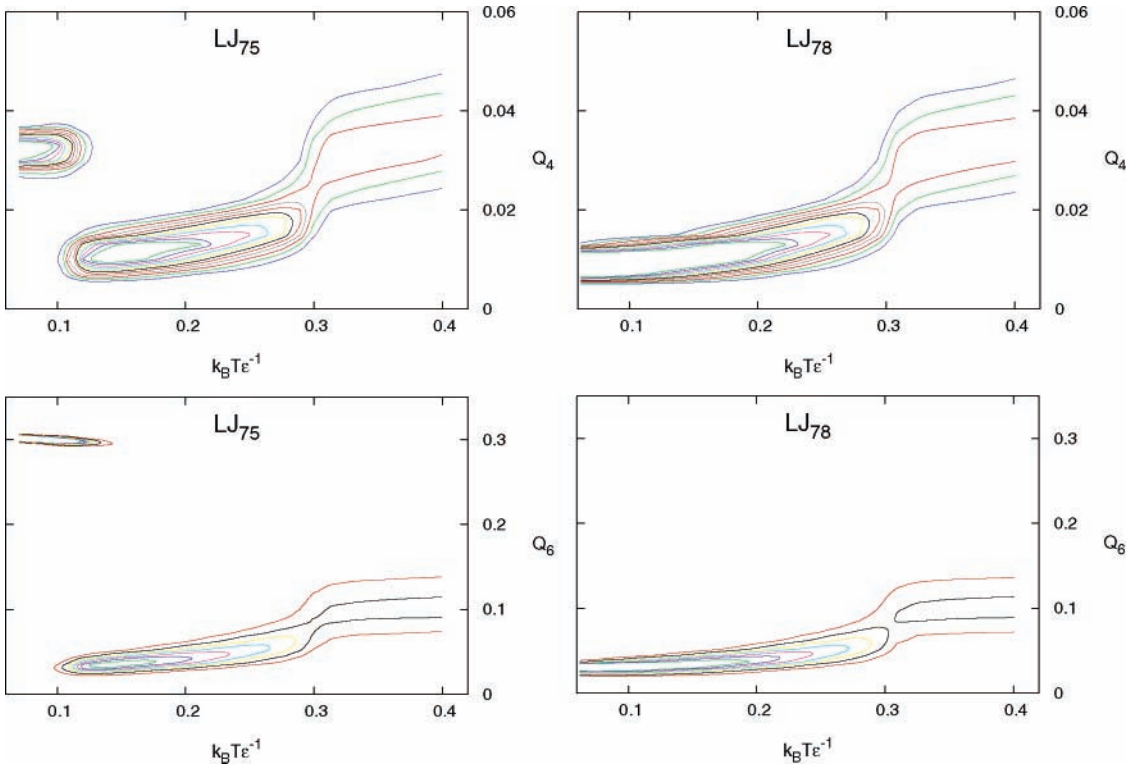


**Figure 6.** Distributions $\rho(T,Q_4)$ (upper panels) and $\rho(T, Q_6)$ (lower panels) of the order parameters $Q_4$ and $Q_6$ for $LJ_{75}$ and $LJ_{78}$. The contour levels of the normalized $\rho(T,Q_6)$ are 7, 14, 21, ..., 49, and those of $\rho(T,Q_4)$ are 20, 30, 40, ..., 120.

The sharp transition between decahedral and icosahedral ground-state structures near $T = 0.11\ \epsilon/k_B$ confirms that the preliminary peak in the heat capacity is the signature of this structural transition. The presence of isomers belonging to the liquidlike class below the melting point shows that these isomers cannot be simply separated according to their energy being lower or higher than the arbitrary threshold of $-394\ \epsilon$. However, the transition toward the liquidlike isomers occurs in a limited temperature range. In contrast to $LJ_{38}$, the transition between the global minimum and icosahedral structures takes place in a narrow temperature range, and there is no overlap between the global minimum and liquidlike isomers, according to our classification. This is mainly due to the larger difference between the two transition temperatures (about $0.2\ \epsilon/k_B$ in the present case, and about $0.05\ \epsilon/k_B$ for $LJ_{38}$[10]).

From our simulations we have also recorded the probability distribution $\rho(T,Q_4)$ and $\rho(T,Q_6)$ of finding configurations with a given $Q_4$ or $Q_6$ as a function of temperature. The assignment of specific values of these order parameters to regions of the energy landscape is made clearer on the two-dimensional contour plots of Figure 6. In addition to the $LJ_{75}$ cluster, we have shown similar data obtained for the purely icosahedral $LJ_{78}$ cluster.

The striking feature of these graphs is the manifestation of the structural transition in $LJ_{75}$ on the disconnected set of regions with nonzero probability. The transition is seen on bimodal distribution of the two order parameters near $T_{ss} \approx 0.11\ \epsilon/k_B$ units. In the case of $LJ_{78}$, the two contour plots show only a single connected region. (We also computed the order parameter distributions for $LJ_{76}$ and $LJ_{77}$, which turned to be qualitatively identical to the case of $LJ_{75}$ and as such are not shown here; consequently, the results for $LJ_{74}$ are qualitatively identical to the case of $LJ_{78}$.)

The $Q_4$ order parameter is not fully appropriate for distinguishing decahedral isomers from liquidlike structures, because all of them are approximately such that $Q_4 > 0.02$. However, the contribution of icosahedral structures only to the lowest values of $Q_4$ is clearly seen in the temperature range 0.1−0.3 for $LJ_{75}$ and $T < 0.3$ for $LJ_{78}$. In this respect, $Q_4$ seems mostly useful for identifying icosahedral isomers. $Q_6$, on the other hand, is more specifically relevant to the decahedral geometries for which it reaches high values. It thus plays a similar role for $LJ_{75}$ as $Q_4$ for $LJ_{38}$. These relations allow us to propose a simple characterization of the three main parts of the energy landscape in terms of their values of the order parameters:

- decahedral minima are such that $Q_6 > 0.2$;
- icosahedral minima are such that $Q_4 < 0.02$;
- liquidlike minima are the remaining isomers.

The probabilities of finding the cluster into one of the three classes according to these definitions does not change significantly with respect to the definition based on quenched energies. These probabilities have been superimposed in Figure 5 to the data obtained from quenching using the open symbols. Although the location of the solid−solid transition is barely affected, the melting transition looks sharper, resembling more the heat capacity of the cluster. Therefore, the $Q_4$ and $Q_6$ order parameters provide a better way of identifying isomers from the two main funnels, and they are also more convenient to uncover disordered liquidlike isomers. However, in contrast to $LJ_{38}$, where $Q_4$ alone was sufficient to achieve this characterization, both $Q_4$ and $Q_6$ are needed for $LJ_{75}$. Incidentally, the requirement of more than one order parameter might hamper the determination of free energy pathways and barriers using conventional simulation techniques.

Before closing this section a few comments about convergence should be addressed. The main heat capacity peak and most of the caloric curve do not vary much once about $1 \times 10^8$ MC steps per replica are used for the calculations. However, the low temperature region is strongly affected by the equilibration time, as shown in Figure 7 for $LJ_{75}$.

The dependence of the calculated heat capacity on the equilibration time follows expected trends.[38] When the simula-

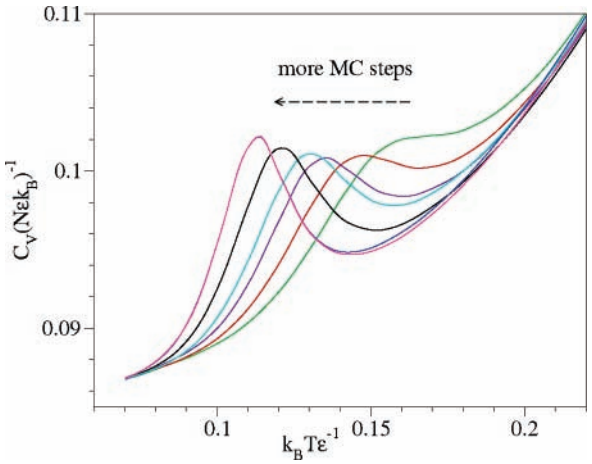


**Figure 7.** Evolution of the low-temperature heat capacity peak for the $LJ_{75}$ cluster (corresponding to the solid−solid transition) during the exchange Monte Carlo simulations. Each of the seven curves has been computed by collecting averages for successive groups of $2 \times 10^9$ MC steps per temperature. The peak gradually shifts to the lower temperatures. The last two curves are hardly distinguishable on the plot. The latter also coincide with that obtained by collecting averages over $1.5 \times 10^{10}$ MC steps after $10^{10}$ equilibration steps.

tion is run shorter, a higher temperature is required to observe as many transitions between metastable states. As the equilibration and/or statistics increase, the peak gets shifted to lower temperatures, and it also gets narrower. The curves shown in Figure 7 do not change significantly once $10^{10}$ MC steps per replica have been performed. As an independent check of our results, we have also tried implementing other temperature schedules with similar numbers of MC steps per replica. Both arithmetic and geometric progressions of 40 temperatures in the range 0.07−0.42 yielded similar curves, although the convergence was slower in both cases, with the geometric schedule being the slowest caused by the lowest replica exchange rate around the melting transition temperature, $T = 0.3$. With the presently available computer resources, equilibration times more than 1 order of magnitude larger than those reported here seem quite out of reach.

Another hint for the convergence of the present results comes from the same ordering between the transition temperatures $T_{ss}$ in $LJ_{75-77}$ as that found from the superposition calculation,[25] $T_{ss}(76) < T_{ss}(77) < T_{ss}(75)$. Also, the proximity of the values of $T_{ss}$ at sizes 76 and 77 is correctly reproduced here. The latent heats $L(n)$ associated with the structural transitions have been estimated from the area of the heat capacity peak. They vary significantly with the cluster size: $L(75) = 8.5\ 10^{-3}\ \epsilon$/atom, $L(76) = 2.1\ 10^{-3}\ \epsilon$/atom, and $L(77) = 4.7\ 10^{-3}\ \epsilon$/atom. The harmonic superposition data of ref 25 give significantly higher values, namely $17 \times 10^{-3}$, $6.5 \times 10^{-3}$, and $8.2 \times 10^{-3}$ for the three clusters $LJ_{75}$, $LJ_{76}$ and $LJ_{77}$, respectively.

The discrepancy between the Monte Carlo calculation and the harmonic superposition data has at least two causes. The first is the possible incompleteness of the samples that represent the two icosahedral and decahedral funnels. In the calculation of ref 25 tens of thousands of minima were included, which makes a strong error unlikely. A probably more severe trouble is the harmonic assumption. Even though the structural transition takes place at rather low temperature, many isomers of the icosahedral or decahedral funnel may be separated from one another by low energy barriers. In such cases the shape of the potential landscape is far from harmonic, and significant variations on the caloric curves may be observed,[37] including shifts in the transition temperatures. As seen in Figure 3 from the strong increase of the heat capacity at temperatures higher than 0.15, the icosahedral phase intermediate between decahedra and the liquidlike state is strongly anharmonic. The neglect of intrinsic anharmonic effects might thus be responsible for a larger part of the difference between the superposition calculation and the present Monte Carlo simulations. Still, we cannot exclude that longer statistics would not slightly shift the heat capacity peaks to lower temperatures. Hence the transition temperatures determined from our simulations should be cautiously considered as upper bounds to the real values.

## IV. Conclusion

Exchange Monte Carlo simulations have been performed for $LJ_n$ clusters in the size range $74 \le n \le 78$. The allocation of temperatures was optimized on the fly, following the procedure described by Hukushima and Nemoto.[33] The five clusters undergo a solidlike−liquidlike phase change near $T = 0.295\ \epsilon/k_B$, with a latent heat $L = 0.20\ \epsilon$/atom. In addition to melting, the clusters with decahedral global minima ($n = 75-77$) exhibit a structural transition toward an icosahedral phase at a lower temperature $T_{ss}(n)$. The present calculations yield $T_{ss}(75) = 0.114\ \epsilon/k_B$, $T_{ss}(76) = 0.065\ \epsilon/k_B$, and $T_{ss}(77) = 0.075\ \epsilon/k_B$. These values are slightly higher than the predictions of the harmonic superposition,[25] even though they are ordered similarly. On the other hand, the associated latent heats are significantly lower than the superposition values but are also ordered similarly with the present MC simulations. Our results emphasize the strong anharmonic behavior of the icosahedral phase, which may explain the quantitative disagreement in the transition temperatures and the latent heats.

As far as atomic clusters are concerned, $LJ_{75}$ seems the natural step beyond $LJ_{38}$ as an application of the EMC method. Other Lennard-Jones clusters with decahedral global minima (at $n = 102-104$) could be interesting as well. $LJ_{98}$, whose tetrahedral global minimum was found only recently,[39] provides another challenge for ergodic simulations. The structural transition between the decahedral or tetrahedral isomers and the icosahedral phase takes place for these clusters at very low temperature ($T_{ss} < 0.02\ \epsilon/k_B$[25]).

The present lack of suitable order parameters makes it more difficult to characterize the structural transition in $LJ_{98}$; hence one would have to rely on thermodynamical quantities only. The success of the EMC on LJ clusters with decahedral global minimum makes it a valuable method for sampling inherent structures and pathways between the two funnels of the energy landscape. Rate constants should then be further evaluated, e.g., from discrete path sampling.[4]

**Acknowledgment.** We thank Prof. D. L. Freeman and Drs. J. P. K. Doye and C. Predescu for fruitful discussions. V.A.M. and P.A.F. acknowledge the NSF support, grant CHE-0414110. V.A.M. is an Alfred P. Sloan research fellow.

## References and Notes

(1) Johnston, R. L. *Atomic and Molecular Clusters*; Taylor and Francis: London, 2002.
(2) Hartke, B. *Angew. Chem.* **2002**, *41*, 1468.
(3) Baletto, F.; Ferrando, R. *Rev. Mod. Phys.* **2005**, *77*, 371.
(4) Wales, D. J. *Mol. Phys.* **2004**, *102*, 883.
(5) Doye, J. P. K.; Wales, D. J.; Berry, R. S. *J. Chem. Phys.* **1994**, *103*, 4234.
(6) Doye, J. P. K.; Miller, M. A.; Wales, D. J. *J. Chem. Phys.* **1999**, *110*, 6896.
(7) Wales, D. J. *Energy Landscapes*; Cambridge University Press: Cambridge, U.K., 2003.
(8) Swendsen, R. H.; Wang, J.-S. *Phys. Rev. Lett.* **1986**, *57*, 2607.

(9) Geyer, C. J. In *Computing Science and Statistics: Proceedings of the 23rd Symposium on the Interface*; Keramidas, E. K., Ed.; Interface Foundation: Fairfax Station, 1991; p 156.
(10) Neirotti, J. P.; Calvo, F.; Freeman, D. L.; Doll, J. D. *J. Chem. Phys.* **2000**, *112*, 10340.
(11) Calvo, F.; Neirotti, J. P.; Freeman, D. L.; Doll, J. D. *J. Chem. Phys.* **2000**, *112*, 10350.
(12) Calvo, F. *J. Phys. Chem. B* **2001**, *105*, 2183.
(13) Frantz, D. D. *J. Chem. Phys.* **2001**, *115*, 6136.
(14) Skone, J. H.; Curotto, E. *J. Chem. Phys.* **2002**, *117*, 7137.
(15) Sabo, D.; Predescu, C.; Doll, J. D.; Freeman, D. L. *J. Chem. Phys.* **2004**, *121*, 856.
(16) Frantsuzov, P. A.; Mandelshtam, V. A. *Phys. Rev. E* **2005**, *72*, 037102.
(17) Predescu, C.; Frantsuzov, P. A.; Mandelshtam, V. A. *J Chem. Phys.* **2005**, *122*, 154305.
(18) Sabo, D.; Freeman, D. L.; Doll, J. D. *J. Chem. Phys.* **2005**, *122*, 094716.
(19) Liu, H.; Jordan, K. D. *J. Phys. Chem. A* **2005**, *109*, 5203.
(20) Calvo, F.; Doye, J. P. K. *Phys. Rev. E* **2001**, *63*, 010902(R).
(21) Doye, J. P. K.; Miller, M. A.; Wales, D. J. *J. Chem. Phys.* **1999**, *111*, 8417.
(22) Doye, J. P. K.; Wales, D. J. *Phys. Rev. Lett.* **1998**, *80*, 1357; *J. Chem. Phys.* **1998**, *109*, 8143.
(23) Wales, D. J. *Mol. Phys.* **1993**, *78*, 151.
(24) Wales, D. J.; Doye, J. P. K. *J. Phys. Chem. A* **1997**, *101*, 5111.
(25) Doye, J. P. K.; Calvo, F. *J. Chem. Phys.* **2002**, *116*, 8307.
(26) Steinhardt, P. J.; Nelson, D. R.; Ronchetti, M. *Phys. Rev. B* **1983**, *28*, 784.
(27) Sugita, Y.; Kitao, A.; Okamoto, Y. *J. Chem. Phys.* **2000**, *113*, 6042.
(28) Kofke, D. A. *J. Chem. Phys.* **2002**, *117*, 6911.
(29) Sanbonmatsu, K.; Garcia, A. E. *Proteins: Struct., Funct., Genet.* **2002**, *46*, 225.
(30) Predescu, C.; Predescu, M.; Ciobanu, C. V. *J. Chem. Phys.* **2004**, *120*, 4119. Kofke, D. A. *J. Chem. Phys.* **2004**, *121*, 1167.
(31) Predescu, C.; Predescu, M.; Ciobanu, C. V. *J. Phys. Chem. B* **2005**, *109*, 4189.
(32) Rathore, N.; Chopra, M.; de Pablo, J. J. *J. Chem. Phys.* **2005**, *122*, 024111.
(33) Hukushima, K.; Nemoto, K. *J. Phys. Soc. Jpn.* **1996**, *65*, 1604.
(34) The Cambridge Cluster Database, http://www-wales.ch.cam.ac.uk/CCD.html
(35) Ferrenberg, A. M.; Swendsen, R. H. *Phys. Rev. Lett.* **1988**, *61*, 2635.
(36) Wales, D. J.; Berry, R. S. *Phys. Rev. Lett.* **1994**, *73*, 2875.
(37) Doye, J. P. K.; Wales, D. J. *J. Chem. Phys.* **1995**, *102*, 9659. Calvo, F.; Doye, J. P. K.; Wales, D. J. *J. Chem. Phys.* **2001**, *115*, 9627.
(38) Calvo, F.; Guet, C. *J. Chem. Phys.* **2000**, *113*, 1315.
(39) Leary, R. H.; Doye, J. P. K. *Phys. Rev. E* **1999**, *60*, R6320.